Measurement of the Hematocrit Using a Paper-Based Microfluidic Device

Samuel Berry

Department of Chemistry, Tufts University

Senior Thesis

April 20th, 2016

Table of Contents

Abstract

The detection and quantification of blood cells provide critical information about a patient's health status. A number of sophisticated instruments, such as hematology analyzers, have been developed to perform these measurements, but limited-resource settings are often lacking the infrastructure required to purchase, operate, and maintain instrumentation. To address the practical difficulties of limited-resource settings, paper-based microfluidic devices have matured as an analytical platform that is capable of performing diagnostic assays in order to provide reliable clinical information. To date, the focus on the use of these tools has been limited to immunoassays, clinical chemistry, and electrochemistry. However, we investigated the use of a paper platform to allow, rather than impede, the flow of cells through paper in order to establish methods for cell assays in paper-based devices. As a proof-of-concept, we developed a paper-based tool for the determination of the hematocrit—the ratio of red blood cell (RBC) volume to total volume of whole blood. We investigated the effects the physical properties of paper had on the device for promoting the transport of RBCs in plasma in paper. The ideal conditions for the fabrication of our device were determined based on our observation of a linear relationship (R^2=0.991) between the lateral distance RBCs traveled and the hematocrit percentage. Our work provides information necessary for overcoming the challenges of developing cell assays in paper-based devices.

Introduction

A critical hematological index—the hematocrit—is the ratio of the packed red blood cell (RBC) volume to the total volume of blood. Hematocrit percentages are values used for many health purposes; in a healthy adult, the hematocrit can range from 36%−48% for women and 42%−52% for men[1]. Deviations from these ranges can be used to determine certain conditions

related to health status, such as dehydration, which is indicated at higher percentages, or anemia, which is indicated in lower percentages in patients.

Hematocrits may be determined using centrifugation. Cells suspended within blood plasma will sediment, stratify, and pack based on their densities upon application of a centrifugal field. Centrifugation results in RBCs packed at the bottom of the sample container (e.g., a capillary tube). The length of the tube occupied by RBCs compared to the total length of the sample in the tube will give the hematocrit percentage. Hematology analyzers can also be used to measure the hematocrit. These instruments count different cell types electronically through impedance measurements and light scattering techniques. In addition to the hematocrit, hematology analyzers can determine other hematological indices (e.g., mean corpuscular volume and leukocyte count) within a given sample. These standard methods for measuring the hematocrit utilize modern and precise technologies and methods in order to provide relevant diagnostic information. However, these established methods are not readily available in limited-resource settings due to the high costs associated with purchase, maintenance, and routine use, thereby impeding the determination of various hematological indices in regions of need.

To address some of the restrictions presented by limited-resource settings, a number of alternative approaches have been developed to analyze samples of blood. Substitute approaches for centrifuges that rely on simple mechanical power have been designed to determine anemia[2] or separate plasma for analysis by clinical chemistry methods.[3] Additionally, rechargeable sources of energy for centrifuges have been used at the point-of-care for the determination of sickle cell disease.[4] Other techniques have been designed to confirm anemia in patients in low-resource settings, but commonly at a high cost.[5,6] These methods supplement established technologies for the use at the point-of-care, but often require additional steps for more complete analyses.

Paper-based microfluidic devices have been explored as an alternative technology for the development of diagnostic assays designed for use at the point-of-care. Paper is an advantageous substrate for point-of-care diagnostic tools for several reasons, such as its ability to store reagents within its matrix and the ability of fluids to flow through paper via capillary action. Paper can also be patterned with hydrophobic barriers and stacked in layers to create three-dimensional networks that direct the flow of fluid and allow for the development of more sophisticated diagnostic assays and devices.[7,8,9,10,11]

Applications of paper-based microfluidic devices have focused on the detection of small molecules or proteins found in urine or plasma to measure liver function, blood glucose concentration, or other diagnostic markers.[12,13,14,15] The cellular component of these samples are removed prior to analysis for several reasons: (i) The grade of paper used to fabricate devices often have small pore sizes (< 11 μm), which can cause cells—with diameters on the order of 6–20 μm—to aggregate or block pores.[16] Cells can thus impede the flow of fluid within a paper-based device, which results in the diminished functionality and reproducibility of assays. Plasma separation membranes are used specifically for this purpose, often coupled with other paper types or in place of paper filters.[17] (ii) The presence of erythrocytes within a paper-based microfluidic device can interfere with any colorimetric assay because of the intrinsic red color caused by hemoglobin.[18]

However, the intrinsic color of red blood cells has been used to derive a colorimetric output for analytical assays. For example, paper-based devices have been developed to determine blood type using channels treated with group-specific agglutinating antibodies (e.g., anti-ABO).[19,20] This approach relies on impeding, rather than enabling, the flow of red blood cells. Others demonstrated that the aggregation of cellular particulates could provide diagnostic

information for sickle cell disease when comparing the radial wicking patterns of lysed red blood cells from healthy and sick patients.[21,22] However, these assays derive health information from the liquid component (e.g., plasma, serum, and cytosol) in samples of blood and are limited in their ability to analyze and screen for properties of intact cells.

By filtering and pretreating the cellular component of these samples, these methods restrict the amount of data and testing that can be obtained from a single sample, disregarding the trove of diagnostic information that can be gleaned from intact, mobile, and viable cells. Therefore, to address these diagnostic limitations, we developed a method that derives clinically relevant information, specifically hematocrit values, from the passage of intact cells through paper. Colloids, such as erythrocytes, require fluid to travel through the fiber network. We use this concept to relate the hematocrit percentage to the wicking of RBCs in paper and the volume of plasma present in the sample, finding the hematocrit percentage to be linearly dependent to the wicking of RBCs.

Materials and Methods

We purchased commercially available Ahlstrom chromatography paper grades 6130 (pore size 6 µm), 54 (pore size 10 µm), and 55 (pore size 15 µm) from Laboratory Sales & Service LLC (Branchburg, NJ). We purchased Whatman grade 4 chromatography paper (pore size 25 µm), citric acid monohydrate, D-(+)-Glucose (45% w/v), dimethyl sulfoxide and 0.5 M ethylenediaminetetraacetic acid (EDTA) from Sigma Aldrich (St. Louis, MO). We purchased sodium chloride from Fisher Scientific. We received trisodium citric acid dihydrate from Amresco. We purchased $DiIC_{18}(3)$ general cell membrane stain from Biotium. We obtained Flexmount Select DF051521 (permanent adhesive-double faced liner) from FLEXcon. We received Jurkat D1.1 cells (CRL-10915) from ATCC. We purchased Fellowes laminate sheets

from Amazon. Isolated RBCs stored in Alsever's solution were obtained from Innovative Research (Novi, MI). Whole blood samples were obtained from Research Blood Components (Brighton, MA).

Fabrication of the paper-based microfluidic device

We designed the hydrophobic barriers that defined the fluidic network in Adobe Illustrator and fabricated the paper layers using a Xerox ColorQube 8580 printer[23]. We assembled the two-layered chromatography paper device using an adhesive sheet that was cut using a Graphtec Cutting Plotter. The exposed area of the second layer was sealed with Fellowes laminate sheets to prevent contamination, evaporation of the sample, and to contain the biological sample within the device. We laminated the completed device with an Apache AL13P laminator.

Treatment of the lateral channel in the paper-based microfluidic device

We applied 40 μL of 50 mM NaCl in 18.2 MΩ DI H_2O (ELGA PuraFlex water purification system) to the top of the lateral channel and allowed the sample to wet the entire channel. Then we dried the layer for 5 minutes at 65 ˚C. We diluted our stock solution of 0.5 M EDTA to a working concentration of 4.5 mM EDTA[24] using 18.2 MΩ DI H_2O. After the lateral channel was treated with NaCl, we added 40 μL of 4.5 mM EDTA in 18.2 MΩ DI H_2O and allowed the sample to completely wet the channel. After, we dried the layer for 5 minutes at 65 ˚C.

Preparation of the samples of hematocrit percentages

Initial hematocrit percentages were determined using standard centrifugation techniques. Briefly, 20 μL of sample was pipetted into a sodium heparin-treated microhematocrit tube, sealed with Critoseal vinyl plastic putty obtained from VWR (Radnor, Pa), and centrifuged at

800 g for 3 minutes. The microhematocrit tube was then scanned using an 8-bit EPSON Perfection V500 PHOTO scanner. The hematocrit of the original sample was calculated by measuring the ratio of the length that RBCs occupied in the tube to the total sample length in ImageJ.[25] We prepared seven hematocrit percentages ranging from 30%–60% by adding or removing plasma depending on the initial hematocrit. To specify, desired hematocrit percentages below the initial hematocrit were diluted using traditional $C_1V_1 = C_2V_2$ (eq.1) where the diluent added was plasma. Hematocrit percentages above the initial hematocrit were obtained by removing an appropriate amount of volume of plasma determined by eq. 2 where *I* is the initial hematocrit fraction, *V* is the volume of sample, *x* is the amount of volume of plasma to remove and *F* is the desired hematocrit fraction.

$$F = \frac{I}{V - x} \qquad \text{eq. 2}$$

Hematocrit percentages were confirmed using standard centrifugation techniques. Prior to adding the samples to the device, they were incubated in a water bath at 37 ˚C for 30 minutes in order to bring the samples up to body temperature. Protocols for RBCs in Alsever's solution and whole blood are similar with the exception that the diluent added to the RBCs is Alsever's solution (42 mg/100 mL NaCl, 80 mg/100 mL Citric acid·3Na·2H_2O, 5.5 mg/100 mL Citric acid monohydrate, and 205 mg/100 mL D-(+)-Glucose in 18 MΩ DI H_2O) unless otherwise stated.

Isolated RBCs suspended in plasma

Seven different hematocrit percentages ranging from 30%–60% using isolated RBCs in Alsever's solution were prepared as previously described. The samples of RBCs were then sedimented and the Alsever's solution was removed from the packed RBCs and that volume was replaced with plasma. Afterwards, the hematocrits were confirmed using centrifugation

techniques. After the samples were prepared, they were incubated at in a water bath at 37 ˚C for 30 minute and then added to the device.

Preparation of WBCs in the hematocrit assay

Jurkat D1.1s, which are human T-lymphocyte, suspension cells, served as a representative cell-type for WBCs in our experiments. D1.1s were cultured in RPMI-1640 media supplemented with 10% fetal bovine serum (FBS) and incubated at 37 ˚C in a 5% CO_2 atmosphere. Samples of D1.1s were prepared in Alsever's solution and concentrations of each sample of D1.1s were confirmed using a Countess (Thermo Fisher).

A sample of isolated RBCs in Alsever's solution with a hematocrit of 48% was prepared. The sample of isolated RBCs was aliquoted into three microcentrifuge tubes and then the RBCs were sedimented, allowing 100 µL of the Alsever's solution to be removed. A 100 µL of the stock solutions of D1.1s in Alsever's solution were added to the samples of isolated RBCs such that the final concentrations of D1.1s in each of the vials were: 1000 cells/µL, 3000 cells/µL, or 5000 cells/µL. After the samples were prepared, they were incubated in a water bath at 37 ˚C for 30 minute and then added to the device.

We used fluorescence microscopy to detect where WBCs travel in the paper-based microfluidic device. We analyzed four paper-based microfluidic devices, each made with a different grade of chromatography paper. We stained the D1.1 cells with a general membrane stain, $DiIC_{18}(3)$, by adding 15 µL of 1 mg/mL $DiIC_{18}(3)$ in DMSO to a 1 mL solution. We incubated the cells for 30 minutes at 37 ˚C in 5% CO_2 atmosphere. The D1.1s were then sedimented at 500 g for 5 minutes and washed twice with fresh RPMI-1640/10% FBS medium. The final concentration of the D1.1s cells was 6000 cells/µL. This concentration was chosen because it is within range of normal concentrations of WBCs found in whole blood.[26] Images

were obtained using a 20X objective on a Leica DMi8 inverted microscope with an Andor DSD2 differential spinning disk confocal unit and Zyla CMOS camera.

Performing and quantifying hematocrit assays on the paper-based microfluidic device

We initiated our assays by applying a 50 µL aliquot of sample to the top layer of our devices. After thirty minutes, we scan the hematocrit devices using the 8-bit EPSON Perfection V500 PHOTO scanner with a resolution of 800-dpi, which we used to convert pixels to inches for our measurements. We measured the distance from the top of the circular zone in the second layer to the farthest edge that the RBCs traveled in the layer. We converted inches to millimeters and analyzed the distances in Microsoft Excel. We subtracted the length of the circular zone and wide channel (15 mm), such that the distances presented were in reference to the thin channel allowing for the results to be resolved qualitatively (i.e., high hematocrits do not enter the thin channel, but normal-low hematocrits do enter the channel).

Experimental Details

Device design

We developed a three-dimensional paper-based device that combines vertical and lateral channels to control and direct the flow of erythrocytes in a sample of applied blood **(Figures 1 and 2)**. Our device is composed of two layers of chromatography paper. The top layer serves as a sample addition layer, which is used to limit white blood cells (WBCs) from entering the channel in the second layer and interfering with the operation of the device (i.e., impeding flow). The bottom layer is designed with a thermometer-styled readout to facilitate the determination of wicking distances. The two layers of chromatography paper are assembled using double-sided permanent adhesive that is cut using a Graphtec cutting plotter. Once assembled, each face of the device is sealed with an adhesive sheet of laminate. The laminate protects the user from

contamination of blood, reduces the evaporation of the sample during the incubation period, and allows a clear field of view to observe the readout.

We investigated several different thermometer-styled readout designs to determine the device that provided the most resolved and reproducible wicking distances for erythrocytes. Ultimately, we designed the lateral channel with segmented elements instead of a single straight channel to permit the wicking of a wide range of hematocrits. To incorporate higher hematocrits (>55%), we designed the channel with an initial wide, short segment that then narrowed into a thinner, longer segment to resolve lower hematocrits (55%-30%). The wide channel (5 x 10 mm) provided sufficient area for a high concentration of cells to migrate into the channel with minimal aggregation caused by a bottleneck effect. Conversely, lower hematocrits—which have larger volumes of plasma— are resolved with a thinner, longer channel (2 x 40 mm) whose dimensions allow for improved lateral wicking of the sample.

We treated the bottom layer of the device with 4.5 mM ethylenediamine tetraacetic acid (EDTA) and 50 mM sodium chloride (NaCl) prior to assembly to further facilitate the wicking of RBCs in our device. The addition of NaCl caused osmotic stress within the RBCs, which improved their wicking distance by decreasing their size and increasing the volume of fluid in the sample. Although the samples of whole blood were treated with anti-coagulant (e.g., sodium heparin or EDTA) by the vendor, the addition of EDTA to the device helped produce a better dynamic range and reproducibility in signal.

Selection of materials

We investigated a range of hematocrit percentages in a common device design, but composed of different commercially available chromatography papers with various pore sizes (i.e., 6 µm, 10 µm, 15 µm, and 25 µm). We compared the dynamic range and precision of each

pore size in order to understand the effect of pore size on particle flow through our device geometry. Fabricating our devices using paper with pore sizes smaller than the diameters of red blood cells (≤ 6 μm) would increase the possibility of aggregation and inhibit the functionality of the device. Indeed, the smaller pore size papers (6-10 μm) restricted the transport of RBCs within the device, although there was wicking of RBCs through this pore size range, which we attribute to the ability of RBCs to deform to smaller sizes (<6 μm)[27,28]. In contrast, paper with larger pore sizes (≥ 25 μm) permits the flow of RBCs but also could allow white blood cells to flow through with an overall lower resolution. We believed that 15 μm would produce the most consistent wicking distances and highest resolution between hematocrits when compared with 6, 10, and 25 μm pore sized papers, being the lowest pore size paper where cells no longer occlude and result in impeded flow. We tested this hypothesis with whole blood **(Figure 3)** on untreated devices of each pore size to see if the sample preferred a specific paper grade. As expected, the 15 μm pore size paper yielded the best results with the optimized treatment and geometry parameters. Lastly, we characterized each choice of chromatography paper with Mercury Intrusion Porosimetry (MIP) in order to determine the pore size distribution of the material.

Analysis of the physical properties of the chromatography paper: pore size distribution

We conducted mercury intrusion porosimetry tests on our 6 μm, 10 μm, 15 μm, and 25 μm papers using a Poremaster 60 Mercury Intrusion Porosimeter from Quantachrome (Boyton Beach, FL). We followed standard MIP protocols for measuring the pore size of each sample. We conducted three replicate tests for the pore size distribution of each paper sample. The 15 μm sample had a median pore size of 13.37 ± 1.14 μm, the 6 μm sample had a median pore size of 15.69 ± 3.56 μm, the 10 μm sample had a median pore size of 19.09 ± .56 μm, and the 25 μm sample had a median pore size of 27.44 ± 6.44 μm. We believe the larger deviations in pore size

from each manufacturer's label are one of the causes of the irreproducibility of the devices made with each paper type, as the 6 µm, 10 µm, and 25 µm all had poor resolution. For each sample pore size, there are pores that are the size labeled by the manufacturing, giving the paper some of the characteristics expected with that pore size (less wicking in the 6 µm, further wicking in the 25 µm), but these pore sizes were not uniform throughout the sample.

Results and Discussion

The measurement of hematocrit, by definition, quantifies the concentration of RBCs in a blood sample. It is often overlooked that the hematocrit also yields information concerning the liquid percentage of the sample, which can be used to predict the hematocrit to the same extent that a packed RBC volume can be. We therefore focused on developing a paper-based diagnostic device that utilized the liquid component as a method of transport for intact RBCs to wick through paper. In order for our device to function, plasma or fluid is needed for cells to wick through the paper. In a 50 µL sample of 50% hematocrit, it is assumed that the wicking distance will be equivalent to that of 25 µL of pure plasma. We applied this basic principle to our initial thermometer-styled device designs (straight channels), and found that pure plasma wicked linearly with respect to the calculated hematocrit percentage **(Figure 4).**

However when we transitioned to a more complex matrix (i.e. whole blood) we experienced decreased reproducibility and dynamic range in our device, indicating that the chemical and physical characteristics of the device needed to be redesigned in order to accommodate whole blood **(Figure 4)**. After comparing multiple device channel dimensions and paper pore sizes, we determined that the segmented channel was an ideal design to promote the wicking of whole blood samples in our device and compared the performance of whole blood and isolated RBCs in this new device design **(Figure 5)**. We observed that the wicking distances

of the isolated red blood cells were greater than the whole blood samples, suggesting that other variables (e.g., plasma content, presence of white blood cells and platelets) could affect the wicking of red blood cells in whole blood. We investigated the influence of these additional variables by examining controlled samples: **(i)** isolated red blood cells in Alsever's solution, **(ii)** isolated red blood cells and cultured white blood cells in Alsever's solution, **(iii)** cultured white blood cells in Alsever's solution, **(iv)** isolated red blood cells resuspended in plasma, and **(v)** plasma. Additionally, we examined the role of device treatment in order to match the wicking capabilities of isolated red blood cells to that of whole blood.

We examined isolated red blood cells and whole blood on devices that were not treated with any additives and on devices treated with NaCl. We compared the performance of each system and observed that the addition of NaCl promoted the reproducible wicking of red blood cells and increased the wicking distance of the sample of whole blood. The NaCl increased the linear correlation coefficient for isolated RBCs in an untreated device from $R^2 = 0.896$ to $R^2 = 0.987$ for isolated RBCs in a NaCl-treated device **(Figure 6).** Although the treatments with NaCl to the lateral channel facilitated wicking of samples of whole blood, we desired a larger dynamic range for our output. This required that we further increase the wicking distances of the lower hematocrits (i.e., < 50% hematocrit percentage).

We chose to treat the lateral channel with an anticoagulant known to decrease the viscosity of plasma, EDTA. We believed that by adding a liquid component to the device, we would be diluting the anticoagulant already present in the sample. By treating the device with EDTA, we are able to reintroduce anticoagulant into the blood sample that may have previously been diluted. The EDTA increased the linear correlation coefficient for EDTA-treated whole blood from $R^2 = 0.957$ for an untreated device and $R^2 = 0.872$ for the NaCl-treated device to $R^2 =$

0.991 for a NaCl/EDTA treated device, as well as increased the dynamic range by 38% **(Figure 7).** However, we still saw a difference in wicking distance when comparing whole blood samples to isolated red blood cells, which we attributed to the liquid component of our samples (i.e., plasma versus Alsever's solution); therefore we probed the influence of plasma in the wicking distances of the samples.

We found the wicking distance of isolated RBCs in Alsever's solution to be 41% greater than the wicking distance of isolated RBCs resuspended in plasma **(Figure 8).** Plasma is more viscous (1.10-1.30 mPa·s)[29] than water (≈.860 mPa·s), leading us to conclude that the change in viscosity decreased the wicking distance of the cells. As determined above, the addition of EDTA to the channel promoted better flow in the plasma-based samples **(Figure 9)** when compared with an untreated device **(Figure 4)**.

The plasma content contributes to the wicking distances by being a liquid medium for cells to travel within the fiber network of the paper; additionally, we examined the influence of white blood cells on the wicking distance of samples of whole blood. We compared the wicking distances of isolated red blood cells with and without white blood cells (WBCs) added to the sample, as well as the wicking distances of cultured WBCs (D1.1 Jurkat cells) in the device. After addition of cultured WBCs in buffer to the device, we found that the buffer wicked to the end of the thermometer channel, indicating that the WBCs did not clog the pores in the paper and impede flow. We then introduced WBCs into our isolated RBC samples, doping these samples with varying levels (1000, 3000, and 5000 cells/μL) of D1.1 Jurkat cells. We imaged the Jurkat cells in paper using a fluorescent probe that stains cell membranes, imaging the positions of the cells on the top layer, and on the top, middle, and bottom of the channel in 6 μm pore size paper, 10 μm pore size paper, 15 μm pore size paper, and 25 μm pore size paper. Microscopy images

(Figure 10) showed that a significant amount of larger cells (i.e., white blood cells) remain on the top layer and no WBCs enter the thin channel of the device**.** These images validate our qualitative assumption derived from the cultured WBCs in Alsever's, indicating that RBCs wick with little interference from WBCs in the thermometer channel. In addition to analyzing the placement of white blood cells in our device using fluorescence microscopy, we verified the presence of intact red blood cells in the lateral channel after staining the red blood cells with a FITC dye conjugated to anti-glycophorin A antibody.

Lastly, we examined blood samples treated with two different anticoagulants, EDTA and sodium heparin (NaHep), to determine if the pretreatment influenced the wicking of the blood in any way. We compared the performance in our device of samples of NaHep treated whole blood and EDTA treated whole blood **(Figures 11 and 12)**. We found that it behaved similarly to the EDTA with a linear correlation coefficients of $R^2 = 0.984$ for the untreated device, $R^2 = 0.930$ for the NaCl-treated device, and $R^2 = 0.985$ for the NaCl/EDTA treated device. Despite these comparable results, we opted to use EDTA-treated whole blood because we found that the biological replicates performed better in the EDTA-treated whole blood than in the NaHep-treated whole blood. One possible explanation for the slight difference between the samples is that the heparin polymers can adhere to cellulose-based materials[30], which may decrease the effective pore size within the paper.

Conclusion

We presented a paper-based microfluidic device that successfully relates the wick distance of a sample of whole blood to the hematocrit of the sample. Unlike other paper-based cell assays[21,22], we do not lyse or pretreat our sample, instead incorporating the intrinsic color and morphological properties of the cell into the function and readout of our device. The passage

of the intact red blood cells through the paper matrix gives us a platform to create an affordable diagnostic device (<$0.03/device) for the measurement of hematocrit at the point-of-care, which decreases diagnostic costs and increases access to health services in this limited resource settings.

Further development of this assay will focus on clinical analysis of blood samples and patients. The heterogeneity of blood samples must be considered in these types of assays where the readout is dependent on wicking distances, as different donors behaved differently in our device **(Figures 13-15)**. Nonhomogeneous biological characteristics between different donors (e.g. blood type, protein content, hydration, etc.) can contribute to these varying results in our assays. Most importantly, the technology we have developed in this device has laid the groundwork for continued expansion in the use of cell-based paper diagnostics. By understanding how particles (e.g. cells) wick through paper, we can create new assays that focus on detection and quantification of cells from complex matrices, providing valuable diagnostic information for a number of conditions.

Acknowledgements

I would like to thank the Tufts Department of Chemistry, the NSF, and the Kanagys for their support in funding this project, Dr. Daniel Schmidt of UMass Lowell for allowing us to use his Mercury Instrusion Porosimeter, and Dr. Kritzer and Dr. Mace for being on my thesis committee. Special thanks to Syrena for helping guide me through this project and everything else for these past few years, and the rest of the Mace Lab for their continued support and inspiration.

References

1. Case Records of the Massachusetts General Hospital: normal reference laboratory values. *N. Engl. J. Med.* **1992**, 327:718-24.
2. J. Brown, L. Theis, L. Kerr, N. Zakhidova, K. O'Connor, M. Uthman, M. Oden, R. Richards-Kortum, *Am. J. Trop. Med. Hyg*. **2011**, *85(2)*, 327.
3. A. P. Wong, M. Gupta, S. S. Shevkoplyas, G.M. Whitesides, *Lab Chip* **2008**, *8*, 2032.
4. A. A. Kumar, M.R. Patton, J. W. Hennek, S.Y.R. Lee, G. D'Alesio-Spina, X. X. Yang, J. Kanter, S. S. Shevkopylas, C. Brugnara, G. M. Whitesides, *Proc. Natl. Acad. Sci. USA* **2014**, *111(41)*, 14864.
5. J.J. Paddle, *Bull World Health Organ.* **2002**;80(10):813–816.
6. E.A.Tyburski, S.E.Gillespie, W.A. Stoy R.G. Mannino, A.J. Weiss, A.F. Siu, R.H. Bulloch, K. Thota, A. Cardenas, W. Session, H.J. Khoury, S. O'Connor, S.T. Bunting, J. Boudreaux, C.R. Forest, M. Gaddh, T. Leong, L.A. Lyon, W. A Lam, *J Clin Invest*. **2014**;124(10):4387-4394.
7. A. W. Martinez, S. T. Philips, G. M. Whitesides, *Natl. Acad, Sci*. **2008**, *105 (50)*, 19606.
8. J. E. Schonhorn, S. C. Fernandes, A. Rajaratnam, R. N. Deraney, J. P. Rolland, C. R. Mace, *Lab Chip*, **2014**, *14*, 4653.
9. A.V. Govindarajan, S. Ramachandran, G.D. Vigil, P. Yager, K.F. Bohringer, *Lab Chip*, **2012**, 12, 174-181.
10. C.M Cheng, A.W. Martinez, J. Gong, C.R. Mace, S.T. Phillips, E. Carrilho, K.A. Mirica, G.M. Whitesides, *Angew. Chem. Int. Ed. Engl.*, **2013** Jun 28;49(28):4771-4.
11. H. Liu, R.M. Crooks, *J. Am. Chem. Soc.*, **2011**, 133(44), 17564-17566.
12. S.J. Vella, P. Beattie, R. Cademartiri, A. Laromaine, A.W. Martinez, S.T Phillips, K.A. Mirica, G.M. Whitesides, *Anal. Chem.*, **2012**, 84(6), 2883-2891.
13. N. R. Pollock, J. P. Rolland, S. Kumar, P. D. Beattie, S. Jain, F. Noubary, V. L. Wong, R. A. Pohlmann, U. S. Ryan, G. M. Whitesides, *Sci. Transl. Med.* **2012** *4*, 152ra129.
14. H.J. Chun, Y.M. Park, Y.D. Han, Y.H. Jang, H.C. Yoon, *Biochip J*, (**2014**) 8(3); 218-226.

15. Z. Nie, C.A Nijhuis, J. Gong, X. Chen, A. Kumachev, A.W. Martinez, M. Narovlyanksy, G.M. Whitesides, *Lab Chip*, **2010**, 10, 477-483.
16. X. Yang, O. Forouzan, T. P. Brown, S. S. Shevkoplyas, *Lab Chip* **2012**, *12*, 274.
17. T. Songjaroen, W. Dungchai, O. Chailapakul, C. S. Henry, W. Laiwattanapaisal, *Lab Chip* **2012**, *12*, 3392.
18. K. Abe, K. Suzuki, D. Citterio, *Anal. Chem.*, **2008**, 80(18), 6928-6934.
19. M.S. Khan, G. Thouas, W. Shen, G. Whyte, G. Garnier, *Anal. Chem*., **2010**, *82*(10), 4158-4164.
20. L.Guan, J. Tian, R. Cao, M. Li, Z. Cai, W.Shen, *Anal. Chem.*, **2014**, 86(22), 11362-11367.
21. X. Yang, J. Kanter, N.Z. Piety, M.S. Benton, S.M Vignes, S.S. Shevkoplyas, *Lab Chip*, **2013**, 13, 1464-1467.
22. N. Z. Piety, X. X. Yang, D. Lezzar, A. George, S. S. Shevkoplyas, *Am. J. Hematol*. **2015**, *90*, 478.
23. E. Carrilho, A.W. Martinez, G.M. Whitesides *Anal. Chem.*, **2009**, 81(16), 7091-7095.
24. H. Sohma, S. Imai, N. Takei, H. Honda, K. Matsumoto, K. Utsumi, K. Matsuki, E. Hasimoto, T. Saito, Y. Kokai, *Front Aging Neurosci*.**2013**; 5: 15.
25. C.A. Schneider, W.S. Rasband, K.W. Eliceiri, *Nat. Methods,* **2012** Jul;9(7):671-5.
26. C.D. Lee, A.R. Folsom, F.J. Nieto, L.E. Chambless, E.Shahar, D.A Wolfe, *Am. J. Epidemiol.*, **2001**, 154(8):758-764.
27. S.S. Shevkoplyas, T. Yoshida, S.C. Gifford, M.W. Bitensky, *Lab Chip*, **2006** Jul;6(7):914-20.
28. E.A. Evans, *Methods Enzymol.*, **1989**; 173:3-35.
29. G. Késmárky, P. Kenyeres, M. Rábai, K. Tóth, *Clin. Hemorheol. Microcirc.* **2008**;39(1-4):243-6.
30. S. Murugesan, J. Xie, R.J. Linhardt, *Curr. Top. Med. Chem.*, **2008**, 8, 80-100.

Figures

Figure 1. Schematic of a paper-based microfluidic device to measure the hematocrit of whole blood. The black regions represent the hydrophobic zones patterned by wax printing and the white regions are the hydrophilic zones of the paper. The layers of adhesive have not been shown for simplicity. After a sample is applied, an incubation period of thirty minutes is required before a readout can be obtained.

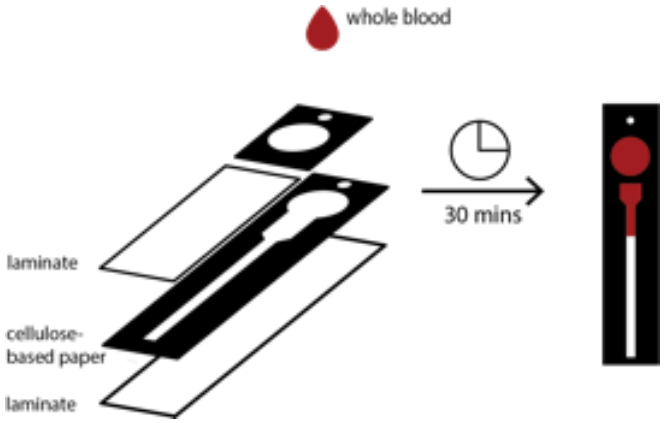

Figure 2. Representative images of paper-based devices at various hematocrit percentages using samples of whole blood.

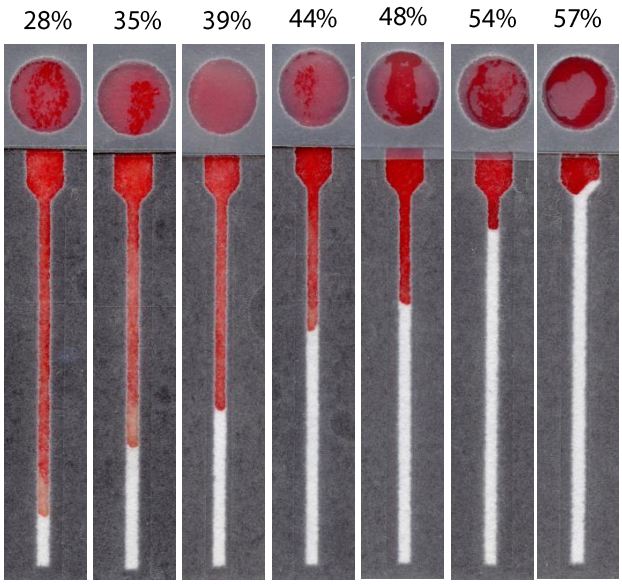

Figure 3. Performance of the hematocrit assay for devices fabricated with chromatography paper with average pore sizes of 6 µm (blue), 10 µm (red), 15 µm (black), and 25µm (grey). No additives were applied to the devices. Each data point represents an average of three replicates and the error bars represent standard error of the mean for each point.

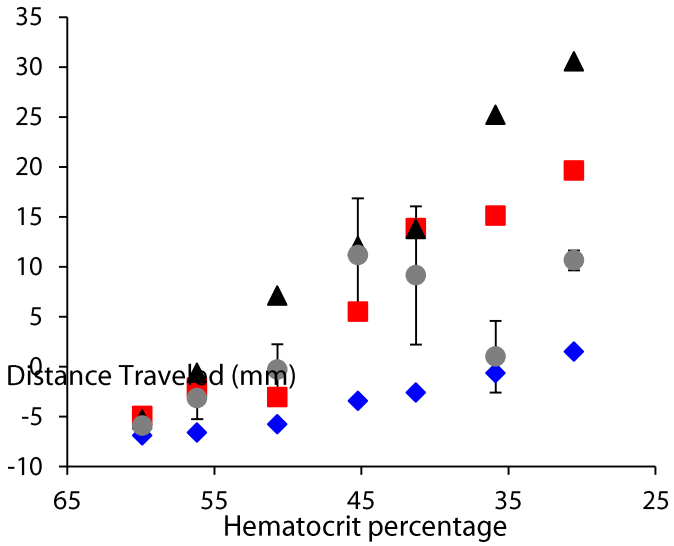

Figure 4. Comparison of the wicking distance for plasma (red) and whole blood (black) samples in the hematocrit device. The devices used in this experiment were not treated with any additives. Each data point represents the average of three replicates for the wicking distance for plasma samples and each data point represents the average of five replicates for the whole blood. The error bars for both data sets represent the standard error of mean.

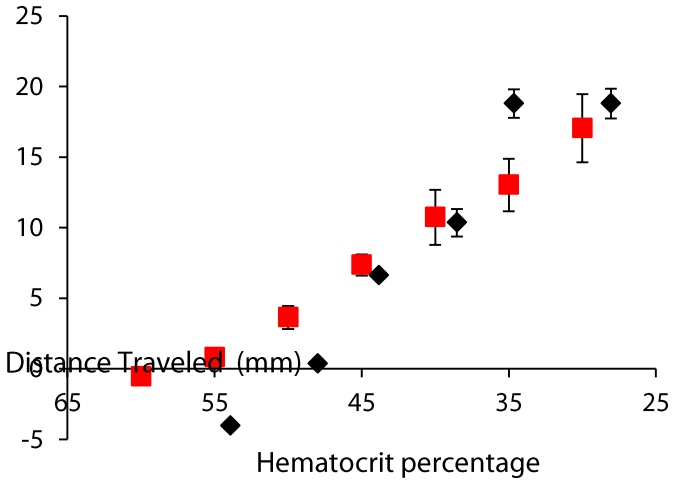

Figure 5. Comparison of the wicking distance for whole blood (red) and isolated RBCs (blue) samples in the hematocrit device. The devices used in this experiment were not treated with any additives. Each data point represents the average of five replicates. The error bars for both data sets represent the standard error of mean.

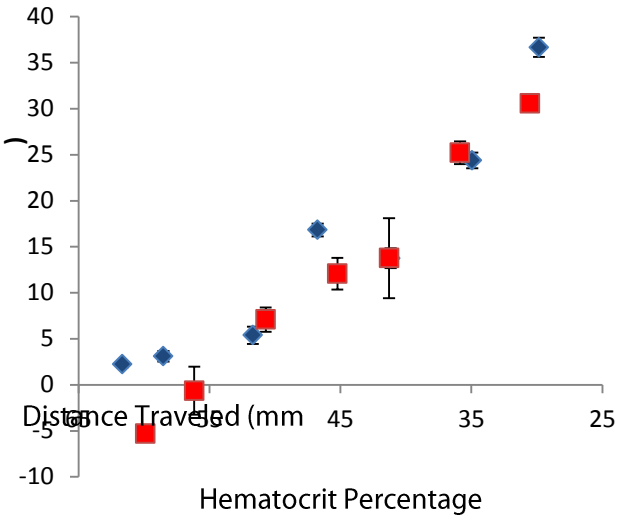

Figure 6. Graphical representation comparing the performance of isolated red blood cells on devices treated with (blue) and without sodium chloride (red). Each data point is the average of five replicates and the error bars represent the standard error of the mean. Each data set is fit to a linear regression line. (with NaCl R^2=0.987, without NaCl R^2=0.896).

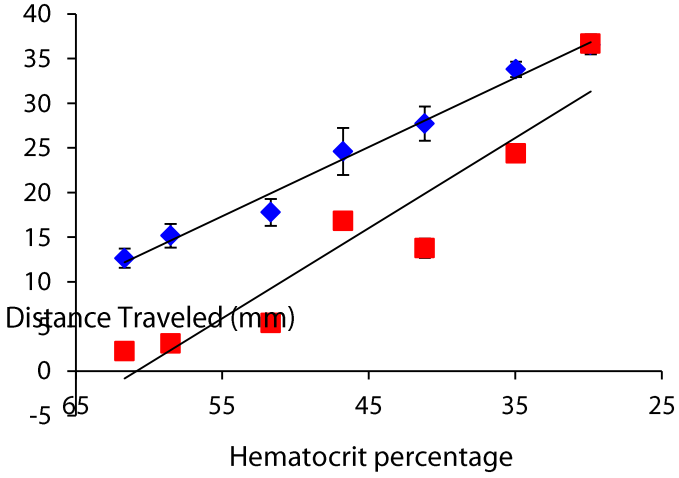

Figure 7. Relationship between hematocrit and wicking distance in a paper-based device. Blood treated with EDTA as anticoagulant. Device treated with NaCl and EDTA to improve wicking. The solid line is the linear fit of the data series (R^2=0.991). Each data point is the average of five replicates and the error bars are standard error of the mean.

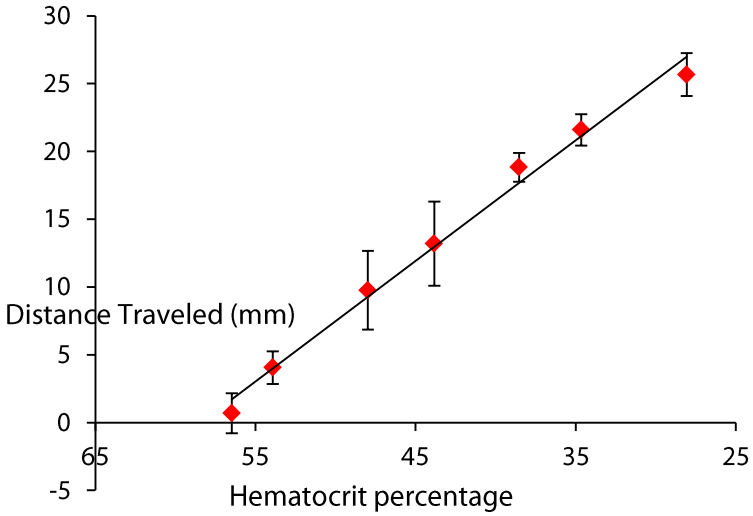

Figure 8. Comparison of the performance of the hematocrit device for samples with various degrees of complexity, RBCs in buffer (blue), isolated RBCs in plasma (red), and whole blood (black). The devices in this experiment were treated with NaCl. Each data point represents the average of five replicates and error bars represent the standard error of the mean for the set.

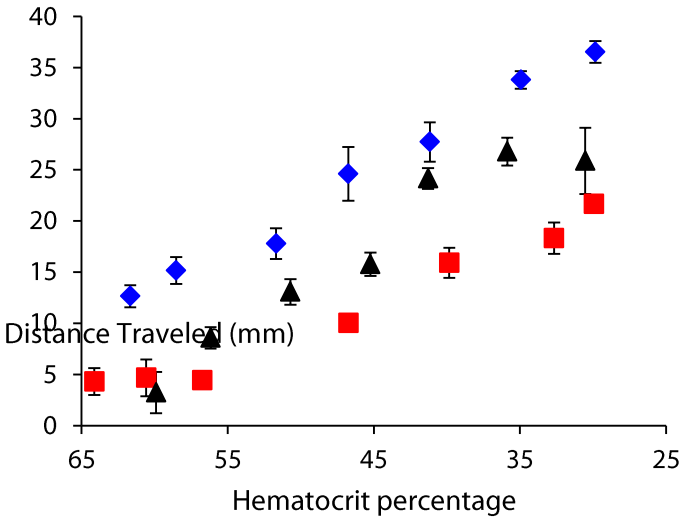

Figure 9. Comparison of the wicking distance for plasma (red) and whole blood (blue) samples in the hematocrit device. The whole blood sample devices used in this experiment were treated with EDTA and NaCl. Each data point for the plasma samples represent the average of three replicates and each data point represents the average of five replicates for whole blood samples. The error bars for both data sets represent the standard error of mean.

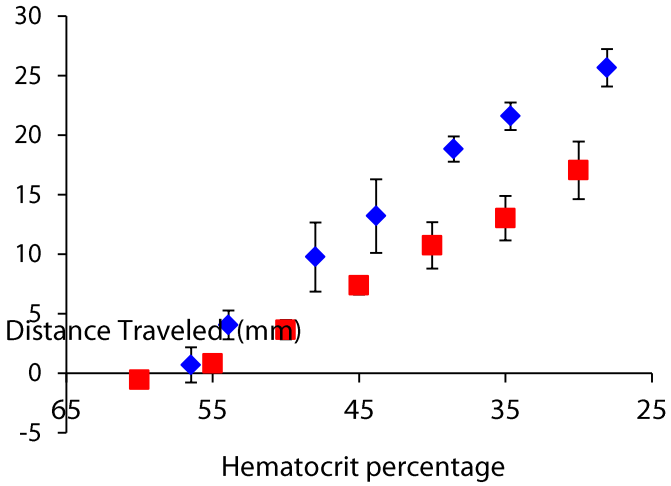

Figure 10. Microscopy images of representative white blood cells stained with $DiIC_{18}(3)$ general cell membrane stain for each grade of paper investigated. (A) Fluorescent images of the circular region of the first layer. (B) Fluorescent images of the circular region (top of the channel) of the second layer. (C) Fluorescent images of the regions the wider channel narrows to the thin channel in the second layer. (D) Fluorescent images of the middle of the thin channel. (E) Fluorescent images of the end of the thin channel.

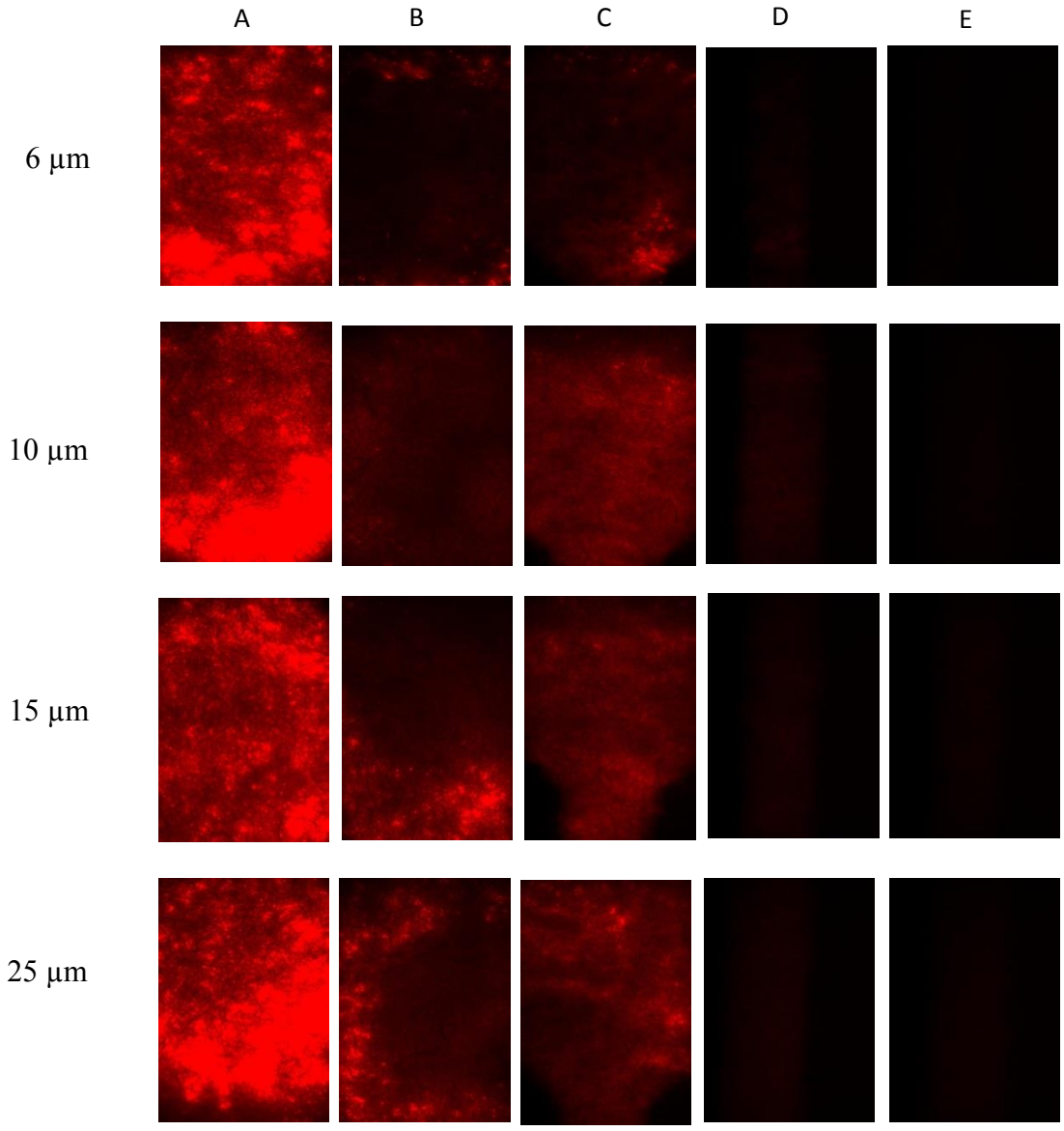

Figure 11. Graphical representation of the performance of hematocrit assays performed on devices: (i) not treated with any additive (blue), (ii) treated with sodium chloride (red), (iii) treated with sodium chloride and EDTA (black) for various hematocrit percentages for samples of whole blood treated with EDTA by vendor. Each data point is the average of five replicates and the error bars are standard error of the mean. The solid line is the linear fit of the data series (no treatment R^2=0.957, NaCl treatment R^2=0.872, NaCl/EDTA treatment R^2=0.991).

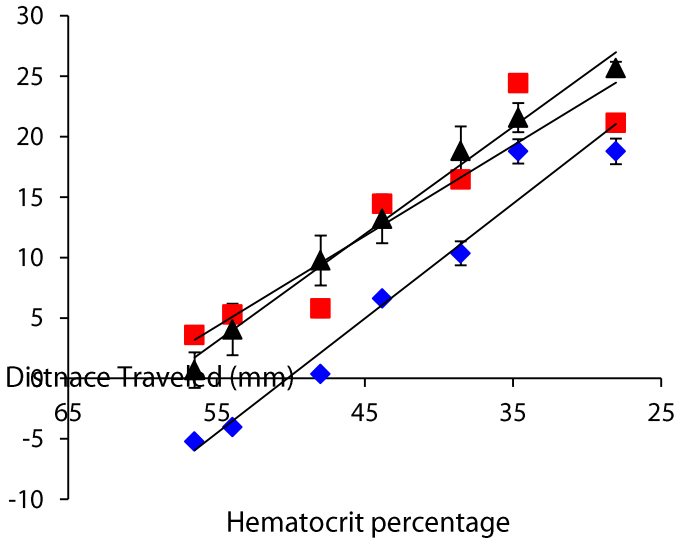

Figure 12. Graphical representation of the performance of hematocrit assays performed on devices: (i) not treated with any additive (blue), (ii) treated with sodium chloride (black), (iii) treated with sodium chloride and EDTA (red) for various hematocrit percentages for samples of whole blood that was treated with sodium heparin by vendor. Each data point is the average of five replicates and the error bars are standard error of the mean. The solid line is the linear fit of the data series (no treatment R^2=0.984, NaCl treatment R^2=0.930, NaCl/EDTA treatment R^2=0.985).

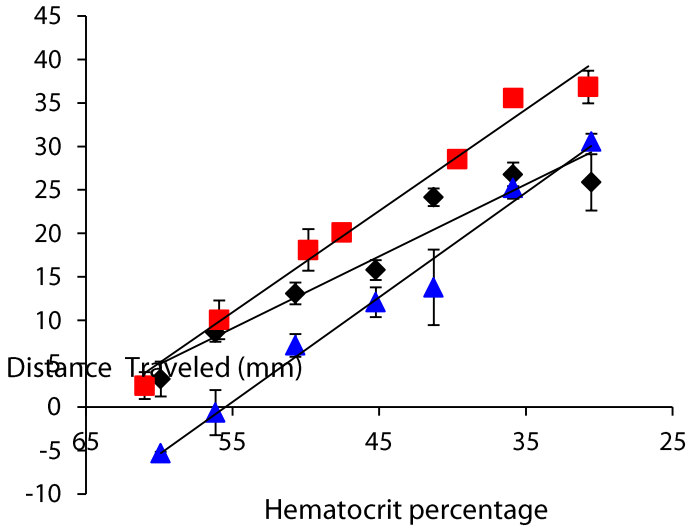

Figure 13. Comparison of the performance of the hematocrit device for different whole blood donors (Donor 1 – blue, Donor 2 – red, Donor 3 – black). The whole blood was treated with EDTA by the vendor. The devices for these experiments were treated with both NaCl and EDTA. Each data point is the average of five replicates and the error bars represent the standard error of the mean.

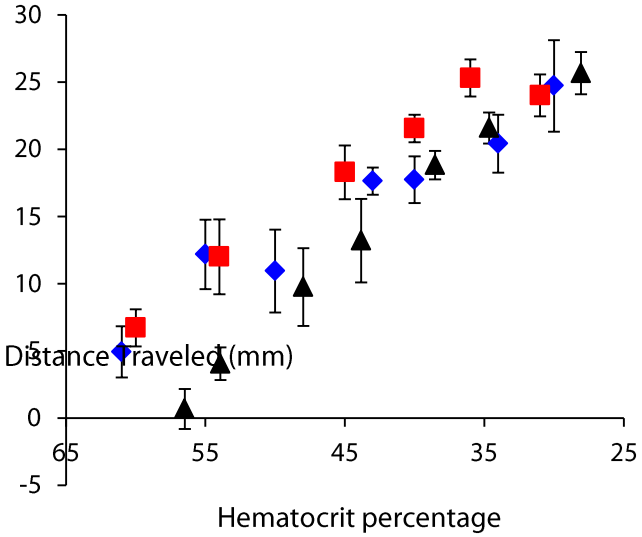

Figure 14. Comparison of the performance of the hematocrit device for different whole blood donors (Donor 1 – blue, Donor 2 – red, Donor 3- black). The whole blood was treated with sodium heparin by the vendor. The devices for these experiments were treated with both NaCl and EDTA. Each data point is the average of ten replicates and the error bars represent the standard deviation.

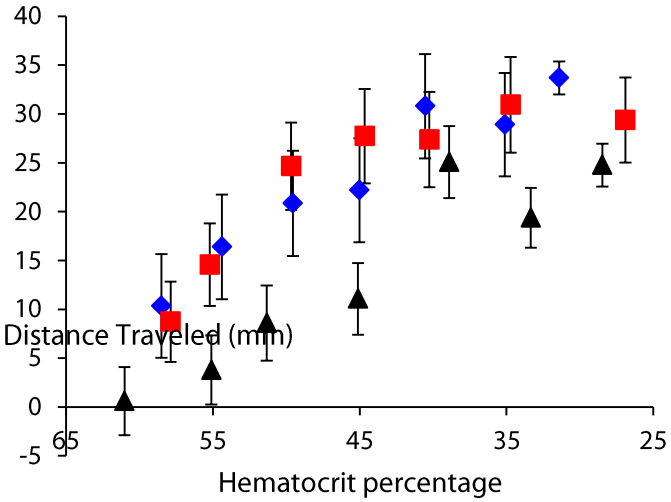

Figure 15. Comparison of wicking distances of plasma from three blood donors (Donor 1-black, Donor 2- red, Donor 3-blue). The devices used in this experiment were not treated with any additives. Each data point represents the average of three replicates and error bars represent the standard error of the mean.